

ELEMENTAL ABUNDANCE DIFFERENCES IN THE 16 CYGNI BINARY SYSTEM: A SIGNATURE OF GAS GIANT PLANET FORMATION?

I. RAMÍREZ¹, J. MELÉNDEZ², D. CORNEJO³, I. U. ROEDERER¹, AND J. R. FISH^{1,4}

To appear in the Astrophysical Journal

ABSTRACT

The atmospheric parameters of the components of the 16 Cygni binary system, in which the secondary has a gas giant planet detected, are measured accurately using high quality observational data. Abundances relative to solar are obtained for 25 elements with a mean error of $\sigma([X/H]) = 0.023$ dex. The fact that 16 Cyg A has about four times more lithium than 16 Cyg B is normal considering the slightly different masses of the stars. The abundance patterns of 16 Cyg A and B, relative to iron, are typical of that observed in most of the so-called solar twin stars, with the exception of the heavy elements ($Z > 30$), which can, however, be explained by Galactic chemical evolution. Differential (A–B) abundances are measured with even higher precision ($\sigma(\Delta[X/H]) = 0.018$ dex, on average). We find that 16 Cyg A is more metal-rich than 16 Cyg B by $\Delta[M/H] = +0.041 \pm 0.007$ dex. On an element-to-element basis, no correlation between the A–B abundance differences and dust condensation temperature (T_C) is detected. Based on these results, we conclude that if the process of planet formation around 16 Cyg B is responsible for the observed abundance pattern, the formation of gas giants produces a constant downwards shift in the photospheric abundance of metals, without a T_C correlation. The latter would be produced by the formation of terrestrial planets instead, as suggested by other recent works on precise elemental abundances. Nevertheless, a scenario consistent with these observations requires the convective envelopes of $\simeq 1M_\odot$ stars to reach their present-day sizes about three times quicker than predicted by standard stellar evolution models.

Subject headings: stars: abundances — stars: fundamental parameters — stars: planetary systems — stars: individual (16 Cyg A, 16 Cyg B)

1. INTRODUCTION

It is often assumed that the members of multiple stellar systems with similar components have the exact same chemical composition since they formed from a common molecular cloud and have undergone similar evolutionary paths. A number of studies have found, however, that elemental abundance differences in binary stars are not uncommon (e.g., Gratton et al. 2001; Laws & Gonzalez 2001; Sadakane et al. 2003; Desidera et al. 2004, 2006). Systematic errors in the spectroscopic analysis could be blamed for some of these anomalies but small differences have been observed even in pairs with very similar components, i.e., in cases where differential analysis is expected to minimize the errors. The origin of these abundance anomalies remains unknown.

Stars and their planets form nearly at the same time. Therefore, it is likely that the process of planet formation leaves detectable signatures in the chemical composition of the host stars. The well-known planet-metallicity correlation in late-type main-sequence stars, for example, suggests that high metallicity increases the probability of forming planets, at least the gas giants (e.g., Marcy et al. 2005; Udry & Santos 2007; Johnson et al. 2010). Meléndez et al. (2009, hereafter M09) have fur-

ther suggested that small anomalies detected in the solar chemical composition compared to that of the majority of so-called solar twin stars, objects with spectra nearly indistinguishable from the solar spectrum, could be due to the formation of terrestrial planets (see also Ramírez et al. 2009, hereafter R09). They detect a small deficiency of refractory elements in the solar photosphere which would disappear if the rocky material that once formed in the solar system were diluted into the present-day solar convective envelope (Chambers 2010). Thus, the missing mass of refractories in the Sun seems to have been locked-up in the rocky bodies of the solar system, including the terrestrial planets.

The hypothesis described above assumes that the formation of the massive gas giants in the solar system did not affect the solar chemical composition, which seems unlikely given the much larger masses of these planets in comparison with the terrestrial planets. Nevertheless, this could be the case if, for example, the abundance ratios of different metals in the gas giants combined were similar to those found in the Sun. Unfortunately, the detailed chemical composition of the gas giants, in particular their cores, is not yet known with enough precision to rule out or confirm this assumption. Careful spectroscopic studies of stars with gas giant planets detected could therefore provide us with important clues about the impact of planet formation on the chemical composition of the host stars.

The binary star 16 Cygni is an ideal system to look for small elemental abundance anomalies and to study the impact of gas giant planet formation. 16 Cyg has long been known as the nearest bound pair of solar twin

ivan@obs.carnegiescience.edu

¹ The Observatories of the Carnegie Institution for Science; 813 Santa Barbara Street, Pasadena, CA 91101, USA

² Departamento de Astronomia do IAG/USP, Universidade de São Paulo; Rua do Mãtao 1226, São Paulo, 05508-900, SP, Brasil

³ Departamento de Astrofísica, Agencia Espacial del Perú CONIDA; Luis Felipe Villarán 1069, San Isidro, Lima, Perú

⁴ Harvey Mudd College; 301 Platt Boulevard, Claremont, CA 91711, USA

stars (e.g., Friel et al. 1993; Porto de Mello & da Silva 1997; Hauser & Marcy 1999), although strictly speaking they should be referred to as solar analogs (cf. Meléndez & Ramírez 2007), in particular because they appear to be older than the Sun. Careful line-by-line differential analysis of this type of stars yields elemental abundances with the highest precision possible, as demonstrated by the works of M09 and R09. Moreover, the components of the 16 Cyg system are bright ($V \sim 6$ mag) and therefore very high quality spectra can be obtained for them using mid-sized telescopes. Thus, extremely high precision differential spectroscopic analysis can be applied to this system.

The secondary star in the 16 Cyg binary system, 16 Cyg B, is known to host a gas giant planet with a minimum mass of 1.5 Jupiter masses ($1.5 M_J$) in a highly eccentric ($e \simeq 0.6$) orbit. Cochran et al. (1997) were the first to detect this planet and they also obtained accurate radial velocity data that showed that 16 Cyg A does not host the same type of planet (gas giant in short-period orbit). Up-to-date follow-up observations of this pair of stars have not changed their planetary status (W. Cochran, private communication). The presence of low-mass and/or long orbital period planets around either of these two stars is, of course, not to be ruled out.

A faint companion, likely a cool M-dwarf, to the primary star 16 Cyg A, at an angular distance of about 3.4 arcsec has been reported by a number of authors (e.g., Hauser & Marcy 1999; Turner et al. 2001; Patience et al. 2002). The absolute magnitude difference between 16 Cyg A and C (the faint companion) is about 8.6 mag in the R band. Their reported separation is large enough for the light from 16 Cyg C to not interfere with that from 16 Cyg A in our data but even if 16 Cyg C was superposed with 16 Cyg A at the time of our observation, it would affect the combined spectrum by less than 0.04 % at $\lambda = 6000 \text{ \AA}$ and even less at shorter wavelengths.

The atmospheric parameters of the 16 Cyg pair have been measured by a number of authors using a variety of techniques. Few of these previous studies, however, present results based on extremely high precision analysis, i.e., significantly better than “standard” methods. One of these studies is that by Laws & Gonzalez (2001), who find that 16 Cyg A is more iron-rich than 16 Cyg B by about $6 \pm 2\%$. They also comment as a note added in proof that a significant positive correlation with dust condensation temperature is found for the abundance difference of 13 elements analyzed. They claim that their results support a self-pollution model in which 16 Cyg A accreted planetary material that once formed there. They also argue that this scenario could explain the observed difference in lithium abundance between 16 Cyg A and B (e.g., King et al. 1997). Later work by Takeda (2005), however, suggests that 16 Cyg A and B have exactly the same chemical composition and attributed the discrepancy with the results by Laws & Gonzalez to differences in the adopted stellar parameters.

Here we derive atmospheric parameters and elemental abundances as precisely and accurately as possible using high quality data of 16 Cyg A and B. High precision elemental abundances are presented for 25 elements in the 16 Cyg binary system. We discuss scenarios that could explain the observed abundance patterns.

2. DATA

The photometric data used in this paper, i.e., magnitudes and colors, correspond to those listed in the General Catalogue of Photometric Data (GCPD, Merrilliott et al. 1997). We adopted the mean values (and errors) given in the GCPD, which have been computed using data from several different sources. For the ($V, B - V$) pair, for example, more than 40 observations from about 10 sources are available for both 16 Cyg A and B.

To calculate the distance to the 16 Cyg system, we adopted the measured trigonometric parallaxes from the latest reduction of Hipparcos data (van Leeuwen 2007). Averaging the published values for the two stars we derive a parallax of 47.29 ± 0.21 mas, which corresponds to a distance of 21.15 ± 0.09 pc.

High resolution ($R = \lambda/\Delta\lambda \simeq 60,000$), high signal-to-noise ratio ($S/N \simeq 300 - 500$, per pixel) spectra were obtained by us with the R. G. Tull coude spectrograph on the 2.7 m Harlan J. Smith Telescope at McDonald Observatory on April 25, 2011. These spectra cover the wavelength region from 4130 to 10 000 \AA , complete up to about 5935 \AA , and with increasingly wider gaps of 2 to 120 \AA towards redder wavelengths. The spectral windows from 6360 to 6440 \AA and from 6480 to 6520 \AA are affected by the so-called “picket fence,” a straylight source of emission lines within the spectrograph (see Sect. 4.6 in Tull et al. 1995), and therefore were not used in this work. Two exposures of 20 minutes each were acquired for both 16 Cyg A and B, one immediately after the other. Data were reduced in the standard manner with the IRAF *echelle* package, using identical reduction parameters for the two stars (e.g., polynomial orders for the overscan and scattered light removal as well as order tracing and aperture widths, flat fields, wavelength solution, etc.). The spectrograph was set so that the $H\alpha$ line at 6562 \AA fell in the center of the detector. This choice was made to properly normalize the $H\alpha$ line profile for effective temperature determination (Sect. 3.3). Continuum normalization was done by fitting high order polynomials to the upper envelopes of each spectral order. Overlapping regions from continuous orders were later merged using the observed counts as weights. The order containing the $H\alpha$ line as well as that containing the $Mg Ib$ lines were normalized differently. For these orders, we took advantage of the smooth variation of the blaze function from one spectral order to the next, to perform a 2D continuum normalization (i.e., both parallel and perpendicular to the direction of dispersion) excluding orders affected by strong lines, as described in Barklem et al. (2002).

Daysky spectra were acquired in the afternoon of April 24, 2011 using the same spectrograph but letting the sky light enter the slit from a “solar port” which points towards the zenith. The data reduction of these spectra, however, was different from that of the stars. Daysky fills up the slit as the source is not point-like. In addition, scattered light in the Earth’s atmosphere is known to affect the line depths and also equivalent widths (e.g., Gray et al. 2000). The latter effect is stronger for large angular separations between the Sun and the area of the sky observed and minimized when the area of the sky observed is very close to the location of the Sun.

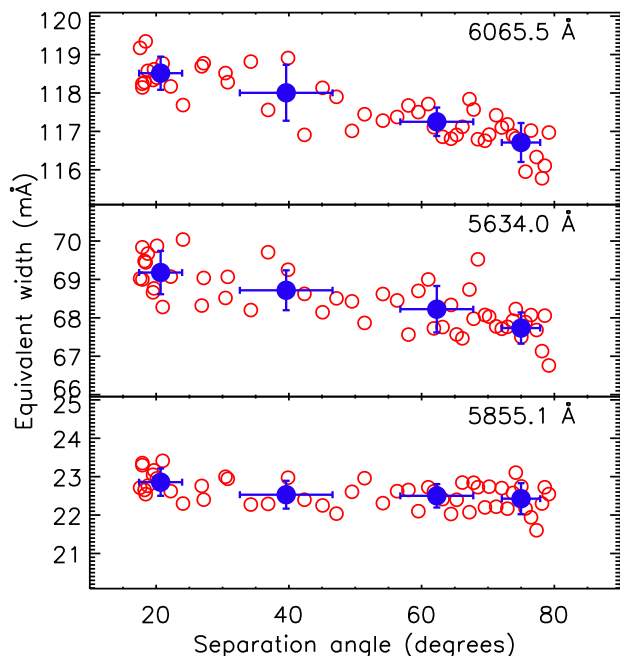


Figure 1. Equivalent widths measured in our daysky spectra as a function of separation angle for three representative lines (open circles). Filled circles with error bars correspond to bin-averaged values.

We obtained daysky spectra for zenith–Sun separation angles from 20 to 80 degrees. The measured equivalent widths clearly correlate with the separation angle (Fig. 1) while the angular variations seem more important for stronger features (Fig. 2). Our daysky spectra reveal the systematic effects described in Gray et al. (2000) and are thus not the best reference for very high precision abundance work. We obtained a number of daysky spectra when the Sun was at its highest point in the sky, about 20 degrees from zenith. Although not ideal, the problems described above are minimized under these circumstances. Thus, our solar reference spectrum corresponds to the average of 10 daysky spectra taken with the Sun near maximum height. We stress that the results obtained using our solar spectrum as reference are expected to be less precise than a differential analysis of 16 Cyg A relative to 16 Cyg B, since the data acquisition and reduction process for the latter are more consistent.

We can use the measurements from Fig. 1 to estimate the error in our measured line equivalent widths (EW s), since the S/N of each of our solar spectra is comparable to that of our 16 Cyg A and B spectra. On average, the error is $\simeq 0.5 \text{ mÅ}$, which corresponds to about 1% for a typical line used in this work ($EW \simeq 50 \text{ mÅ}$).

We compiled a long list of spectral lines for the elemental abundance determination. Due to the differential nature of our work, and the similarity of the two brightest stars in the 16 Cyg system, as well as their similarity to the Sun, accurate atomic data are not strictly necessary. We started with the linelist used by Asplund et al. (2009, hereafter A09), which was carefully constructed for their solar abundance analysis. Not only are these lines mostly free from severe blends but also their atomic data are accurately known. We complemented the iron linelist with the compilation by Ramírez et al. (2007, hereafter R07), which consists of

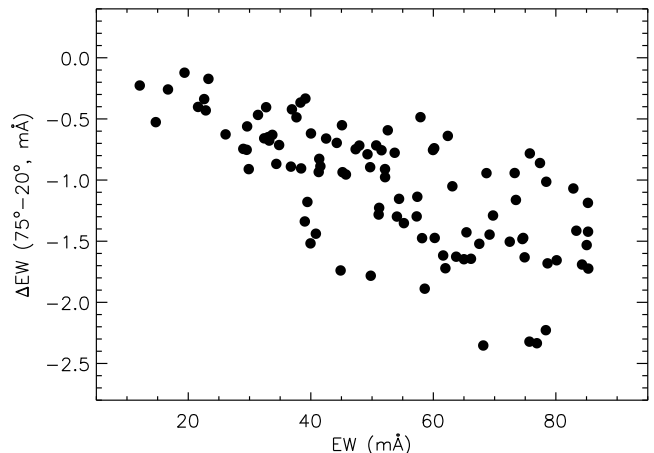


Figure 2. Equivalent width difference measured in our solar spectra at 75 degrees minus 20 degrees of separation angle as a function of the equivalent width measured at 20 degrees of separation angle. Bin-averaged EW s (cf. Fig. 1) were used in this figure.

lines that appear mostly unblended in solar-type stars and have reasonably accurate atomic data measured in the laboratory. For the rest of elements studied in this paper, we used additional lines listed in other large studies of solar-type stars: Reddy et al. (2003, hereafter R03), Bensby et al. (2005, hereafter B05), Neves et al. (2009, hereafter N09), and M09. Our adopted linelist is given in Table 1, along with the source from which atomic data were adopted. When available, we used the van der Waals damping constants by Barklem et al. (2000) and Barklem & Asplund-Johansson (2005), otherwise we adopted the values obtained from Unsöld’s approximation but with the C_6 constants (e.g., Gray 1992, page 217) multiplied by a factor of 3.1, a number that we estimated empirically from a study of the lines that are included in Barklem’s work.

Spectral line equivalent widths (EW s) were measured interactively using the `splot` task in IRAF. The locations of the local continuum, which are crucial for precise measurements of EW , were selected as carefully as possible. For each line, we searched for regions clearly free from spectral lines in the three spectra: solar, 16 Cyg A and B. The exact same wavelengths for the continuum were used for all three spectra. If a small blend appeared to affect only one of the line wings, the other wing was used to measure EW by fitting only that side of the spectral line to a Gaussian profile. This procedure tends to result in more precise EW values than deblending the line because of the uncertainty in determining the core wavelength of the blend. In these cases, we also ensured that the local continua for all three spectra were chosen as similarly as possible. We excluded features affected by telluric absorption.

Equivalent width analysis allowed us to measure abundances of 22 elements: C, O, Na, Mg, Al, Si, S, K, Ca, Sc, Ti, V, Cr, Mn, Fe, Co, Ni, Cu, Zn, Y, Zr, and Ba but we also measured abundances of the heavy elements Nd and Eu. Most of the Nd II and Eu II features are very weak and heavily blended in solar-type spectra. Thus, spectrum synthesis was necessary to measure their abundances. To ensure high precision, we restricted our analysis to the best lines available, i.e., those with a very good continuum normalization and clearly identified blends

Table 1
Adopted atomic data and our measured equivalent widths.

λ (Å)	species	EP (eV)	$\log(gf)$	source	EW (mÅ)	EW (mÅ)	EW (mÅ)
					16 Cyg A	16 Cyg B	Sun
5052.1670	C	7.685	-1.304	A09	40.0	35.7	34.7
5380.3369	C	7.685	-1.615	A09	27.2	23.8	22.7
7771.9438	O	9.146	0.352	A09	82.6	74.8	71.9
7774.1611	O	9.146	0.223	A09	71.5	65.5	62.5
7775.3901	O	9.146	0.002	A09	57.1	51.7	48.6
6160.7471	Na	2.104	-1.246	A09	61.2	61.5	55.9
4730.0400	Mg	4.340	-2.390	R03	75.9	76.3	69.1
5711.0879	Mg	4.345	-1.729	A09	111.6	112.3	107.8
6318.7168	Mg	5.108	-1.945	M09	45.2	44.4	43.7
6319.2368	Mg	5.108	-2.324	A09	31.6	30.1	25.0
6696.0181	Al	3.143	-1.481	A09	48.4	47.9	40.5
6698.6670	Al	3.143	-1.782	A09	25.9	26.7	21.2
5665.5542	Si	4.920	-1.940	M09	48.6	47.7	41.9
5517.5400	Si	5.080	-2.496	N09	17.6	16.6	13.7
5690.4248	Si	4.930	-1.773	A09	60.0	58.0	52.0
5701.1050	Si	4.930	-1.953	A09	46.0	44.8	38.8
5772.1450	Si	5.082	-1.653	A09	60.2	58.1	53.8
5793.0732	Si	4.930	-1.963	A09	52.2	50.1	45.6
5948.5400	Si	5.080	-1.208	N09	94.5	92.6	90.0
6125.0298	Si	5.610	-1.510	R03	39.3	37.5	32.8
6142.4902	Si	5.620	-1.540	R03	38.3	37.5	32.3
6145.0200	Si	5.610	-1.480	R03	47.8	45.1	39.6
6237.3301	Si	5.610	-1.116	N09	73.6	71.4	65.1
6244.4800	Si	5.610	-1.360	R03	55.7	54.7	48.1
6721.8398	Si	5.863	-1.060	R03	55.7	54.0	47.4
7405.7700	Si	5.614	-0.720	B03	101.4	99.2	94.8
7800.0000	Si	6.180	-0.710	R03	64.7	60.1	58.6
4695.4429	S	6.525	-1.829	A09	9.5	8.2	7.1
6743.5400	S	7.866	-0.600	M09	10.1	8.4	8.3
...

with proper modeling and atomic parameters. We analyzed 2 Eu II lines (4205 and 6645.10 Å) and 3 Nd II lines (5293.16, 5319.81, and 5811.57 Å). For Eu we adopted the following isotopic fractions: $^{151}\text{Eu} = 0.478$ and $^{153}\text{Eu} = 0.522$ (e.g., Lodders 2003). The relevant laboratory data used (transition probabilities, isotopic shifts, etc.) are given by Den Hartog et al. (2003), Lawler et al. (2001), Ivans et al. (2006), and Roederer et al. (2008). Finally, lithium abundances were derived using line synthesis of the 6708 Å Li doublet, as described in Baumann et al. (2010).

3. ATMOSPHERIC PARAMETERS

The results presented in this section were obtained using the grid of MARCS model atmospheres (Gustafsson et al. 2008) available online.⁵ Tests made with different flavors of Kurucz’ model atmospheres show that the choice of atmospheric models has a very minor impact on our derived relative parameters and abundances. We comment briefly on these effects in later sections of this paper. Curve-of-growth analysis was used to measure elemental abundances from our equivalent width measurements using the 2010 version of the spectrum synthesis code MOOG (Snedden 1973).⁶ Line profile fitting was used to better constrain T_{eff} from the H α line and $\log g$ from the Mg I b lines. For the former, we used a fine grid of H α theoretical line profiles (steps of 10 K in T_{eff} , and 0.05 dex in $\log g$ and [Fe/H]), computed as

in Barklem et al. (2002).⁷ Finally, the synthesis of the Mg I b lines was done using SYNSPEC (Hubeny 1988; Hubeny & Lanz 1995).⁸

Stellar parameters often depend on each other so the process of their determination is intrinsically iterative. Here we present results which are self-consistent, in the sense that when we “adopt” a value below in the calculation of a given parameter, we have made sure that no further changes to any of the other parameters involved will occur after another iteration.

3.1. Excitation/ionization equilibrium

The iron lines alone can be used to determine the atmospheric parameters using the conditions of excitation and ionization equilibrium. We start by assuming that the atmospheric parameters T_{eff} (effective temperature), $\log g$ (surface gravity), [Fe/H] (iron abundance),⁹ and v_t (microturbulent velocity) of 16 Cyg A and B are solar (i.e., $T_{\text{eff}}, \log g, [\text{Fe}/\text{H}], v_t = 5777 \text{ K}, 4.437, 0.00, 1.00 \text{ km s}^{-1}$).¹⁰ Then, T_{eff} and v_t were iteratively modified so that trends of iron abundance (from Fe I lines only) with excitation potential

⁷ These H α profiles were also computed using MARCS atmospheric models.

⁸ <http://nova.astro.umd.edu/Synspec43/synspec.html>

⁹ We use the standard notation: $A_X = \log(n_X/n_H) + 12$, where n_X is the number density of element X, and $[X/H] = A_X - A_X^\odot$.

¹⁰ The solar microturbulent velocity v_t is somewhat uncertain and dependent on the iron line list used and model atmosphere adopted. Its exact value is not crucial for our strictly differential study, as shown later.

⁵ <http://marcs.astro.uu.se>

⁶ <http://www.as.utexas.edu/~chris/moog.html>

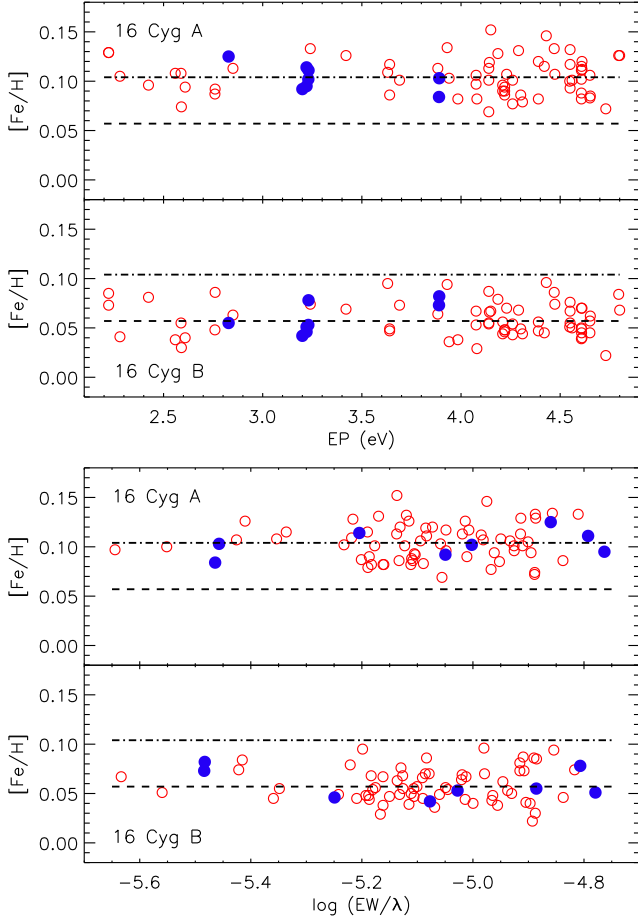


Figure 3. Top panels: $[\text{Fe}/\text{H}]$ values determined on a line-by-line basis with respect to our solar spectrum as a function of excitation potential for 16 Cyg A and B; Fe I (Fe II) lines are shown with open (filled) circles. The dot-dashed line is at $[\text{Fe}/\text{H}] = +0.104$ while the dashed line is at $[\text{Fe}/\text{H}] = +0.057$, which are the mean $[\text{Fe}/\text{H}]$ values for 16 Cyg A and B, respectively. Bottom panels: as in the top panels but as a function of reduced equivalent width.

(EP) and reduced equivalent width ($\log EW/\lambda$), respectively, approached zero. Simultaneously, $\log g$ was modified so that the mean difference in iron abundance from Fe I and Fe II lines also approached zero. Errors in the derived parameters were computed from the uncertainty in the measured slope of abundance versus EP (for T_{eff}) and from the standard deviation of the mean difference of Fe I and Fe II abundances (for $\log g$).

Using the excitation/ionization equilibrium method we obtain: $T_{\text{eff}} = 5818 \pm 38 \text{ K}$, $\log g = 4.31 \pm 0.05$, $[\text{Fe}/\text{H}] = +0.104 \pm 0.018$ for 16 Cyg A; and $T_{\text{eff}} = 5742 \pm 30 \text{ K}$, $\log g = 4.31 \pm 0.05$, $[\text{Fe}/\text{H}] = +0.057 \pm 0.017$ for 16 Cyg B (see Fig. 3). If we use Kurucz no-overshoot models instead of MARCS we find a shift of only $+5 \text{ K}$ in T_{eff} , $+0.01 \text{ dex}$ in $\log g$, and $+0.002 \text{ dex}$ in $[\text{Fe}/\text{H}]$, systematically consistent for both stars. Moreover, adopting a slightly different solar microturbulence: $v_t = 1.0 \pm 0.1 \text{ km s}^{-1}$, we find changes of only $\pm 0.003 \text{ dex}$ in $[\text{Fe}/\text{H}]$ and, as expected, shifts of $\pm 0.1 \text{ km s}^{-1}$ in the microturbulent velocities of 16 Cyg A and B. This shows that the choices of model atmosphere flavor and solar microturbulence have an almost negligible impact on our differential abundance results.

The calculation described in this section suggests that

16 Cyg A is slightly more metal-rich than 16 Cyg B. However, since there is a non-negligible difference in the effective temperature of the stars, small differential systematic effects might still be present and it is therefore important to check the parameters here derived using other independent methods.

3.2. Photometric effective temperature

Casagrande et al. (2010) have implemented the so-called infrared flux method (IRFM) to derive the effective temperatures of a large sample of dwarf and subgiant stars. The zero point of their temperature scale has been determined with an unprecedented precision of only 15 K. Metallicity-dependent color- T_{eff} transformations provided in that work allow us to estimate T_{eff} values for the 16 Cyg A and B pair from their observed photometry. We used the $(B - V)$ and $(b - y)$ colors and our derived $[\text{Fe}/\text{H}]$ values to obtain: $T_{\text{eff}} = 5792 \text{ K}$ for 16 Cyg A and $T_{\text{eff}} = 5733 \text{ K}$ for 16 Cyg B. Photometric errors translate into an error of about 16 K for both stars, similar to the color-to-color error. The uncertainties in $[\text{Fe}/\text{H}]$ translate into a 5 K uncertainty in T_{eff} . Adding these errors in quadrature we estimate a random error of 23 K, which has to be added linearly to the systematic error in the zero point of the Casagrande et al. (2010) T_{eff} scale to estimate the uncertainties in our derived T_{eff} values. Thus, the effective temperatures we derived using colors have errors of 38 K.

The color temperatures, which are based on the most reliable IRFM temperature scale to date, confirm that 16 Cyg A is warmer than 16 Cyg B, although the difference seems to be smaller when using the IRFM T_{eff} scale (59 K) instead of the spectroscopic method described in the previous section (76 K). Nevertheless, the T_{eff} values from the two methods are in good agreement within the 1σ errors.

3.3. Model fits to the $\text{H}\alpha$ line profile

The wings of the Balmer lines are known to be sensitive to T_{eff} and if $\log g$ and $[\text{Fe}/\text{H}]$ can be estimated with high precision independently, as in our case, model fits to the $\text{H}\alpha$ line profile can provide very precise T_{eff} values (e.g., Fuhrmann et al. 1994; Barklem et al. 2002; Ramírez et al. 2006). This is particularly the case if a good continuum normalization is made using very high quality spectra.

We used least squares minimization to find the best model fits to our $\text{H}\alpha$ data as well as the formal errors in T_{eff} . Careful inspection of our spectra allowed us to find several wavelength windows free from spectral lines, both stellar and telluric, other than $\text{H}\alpha$, which were then used in the model fits. The same windows were used for the three spectra. In Fig. 4 we show the observed normalized $\text{H}\alpha$ lines for 16 Cyg A, B, and the Sun (daysky) along with their best fit models. The problems described in Sect. 2 for the solar spectrum are not as important for this broad feature, in particular because we are only interested in the wings, so we can use reliably our daysky spectrum as solar reference in this case. For our solar data, we derive $T_{\text{eff}} = 5732 \pm 32 \text{ K}$, similar to the value obtained by Barklem et al. (2002).¹¹ This suggests that

¹¹ Our error bar here corresponds to observational noise only.

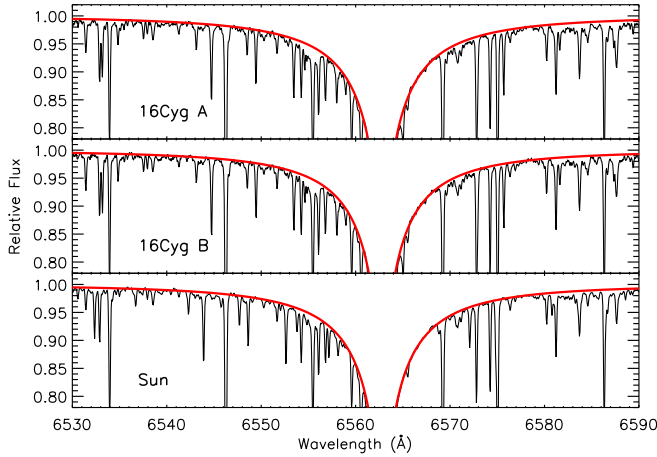


Figure 4. Observed normalized $H\alpha$ line profiles in our 16 Cyg A, 16 Cyg B, and daysky (Sun) spectra. Best fit models for these lines are also shown.

there is still room for improvement in the modeling of Balmer lines. Hereafter, we apply a zero point correction of +45 K to the effective temperatures derived from $H\alpha$ since this brings our derived solar T_{eff} up to the nominal value of 5777 K.

We computed T_{eff} values from the $H\alpha$ line profile fits for a small grid of $\log g = 4.2, 4.3, 4.4$ and $[\text{Fe}/\text{H}] = 0.00, 0.05, 0.10$. Then, we used the grid of T_{eff} results to interpolate to our preferred $\log g$ and $[\text{Fe}/\text{H}]$ parameters as well as to compute the error introduced by uncertainties in $\log g$ and $[\text{Fe}/\text{H}]$. With our final $\log g$ and $[\text{Fe}/\text{H}]$ values we obtain: $T_{\text{eff}} = 5819 \pm 25$ K for 16 Cyg A and $T_{\text{eff}} = 5762 \pm 26$ K for 16 Cyg B. An error of 0.02 dex in $\log g$ translates into only 2 K whereas an error of 0.03 dex in $[\text{Fe}/\text{H}]$ translates into about 1 K of T_{eff} . The uncertainties in our derived values of $\log g$ and $[\text{Fe}/\text{H}]$ thus have negligible impact on this calculation. Moreover, given the very high signal-to-noise ratios of our spectra in this region ($S/N \simeq 500$, obtained because the spectrograph setup was chosen to maximize S/N at 6562 Å), our T_{eff} values derived from $H\alpha$ line profile fitting are the most reliable, as the smaller errors in comparison with T_{eff} values derived with other methods suggest.

Our three estimates of T_{eff} are in excellent agreement with each other for both 16 Cyg A and B. Since these techniques are independent, we can obtain a final T_{eff} value by averaging them, using the estimated errors as weights. We find: $T_{\text{eff}} = 5813 \pm 18$ K for 16 Cyg A and $T_{\text{eff}} = 5749 \pm 17$ K for 16 Cyg B.¹² The degree of precision with which we have been able to measure the effective temperatures of these stars is almost unprecedented for

Barklem et al. (2002) studied systematic errors very carefully and obtained an error of about 80 K for their solar analysis. To remain consistent with the rest of our strictly differential work, we consider the observational errors only.

¹² We calculate the weighted mean value (x) and error (σ) of N data points x_i with errors σ_i as follows: $x = \sum(x_i/\sigma_i^2)/\sum(1/\sigma_i^2)$, $\sigma^2 = 1/\sum(1/\sigma_i^2)$. We note, however, that this formula for σ does not take into account possible systematic errors and could also under- or over-estimate the error if the σ_i values are not realistic. The error computed from the sample variance is in principle more reliable: $\sigma^2 = \{\sum[(x_i - x)^2/\sigma_i^2]/\sum(1/\sigma_i^2)\}/(N - 1)$. Using the latter we find T_{eff} errors of 8 and 9 K for 16 Cyg A and B, respectively, but we adopt the former, more conservative error bars.

any other star but the Sun. The only other exception is the case of the solar twin star HIP 56948, for which Meléndez et al. (2011) report a T_{eff} with an error of 7 K.

3.4. Trigonometric surface gravity

The parallax of the 16 Cyg pair has been accurately measured by the Hipparcos mission (Perryman et al. 1997). The new reduction by van Leeuwen (2007) gives values of 47.44 ± 0.27 mas for 16 Cyg A and 47.14 ± 0.27 mas for 16 Cyg B. The V magnitudes of these stars are also precisely known: $V(\text{A}) = 5.959 \pm 0.009$, $V(\text{B}) = 6.228 \pm 0.019$. Using these numbers we can infer the absolute V magnitudes of the stars: $M_V(\text{A}) = 4.340 \pm 0.015$, $M_V(\text{B}) = 4.595 \pm 0.023$. Since their effective temperatures are also known with very high precision, we can reliably place the stars on the HR diagram and compare their location with theoretical stellar evolution predictions (isochrones) to infer their masses, ages, and surface gravities.

Our particular implementation of stellar parameter determination using isochrones is described in Meléndez et al. (2011, see also Baumann et al. 2010). Our method follows the probabilistic scheme explained in R03 (their Sect. 3.4) and also Allende Prieto et al. (2004, their Appendix A) but the choice of isochrones is different. Basically, all isochrone points within a radius of 3σ from the observed parameters are used to compute mass, age, and $\log g$ probability distribution functions, from which a most likely value and 68% (1σ -like) and 95% (2σ -like) confidence limits can be derived. Finely spaced Yonsei-Yale isochrones (e.g., Yi et al. 2001, 2003; Kim et al. 2002) were used in these computations.

Using our isochrone method we infer masses of $M(\text{A}) = 1.05 \pm 0.02 M_{\odot}$ and $M(\text{B}) = 1.00 \pm 0.01 M_{\odot}$. For the surface gravities we find: $\log g(\text{A}) = 4.28 \pm 0.02$ and $\log g(\text{B}) = 4.33 \pm 0.02$. Since the two stars were born at the same time, it is expected for the primary to be slightly more evolved given its somewhat larger mass.

The ages that we infer for the stars in the 16 Cyg system are: $\tau(\text{A}) = 7.15^{+0.04}_{-1.03}$ Gyr and $\tau(\text{B}) = 7.26^{+0.69}_{-0.33}$ Gyr. Error bars correspond to the 1σ -like lower and upper limits. The age probability distributions (APDs) for these stars are shown in Fig. 5. The asymmetry of these APDs explains the very different upper and lower 1σ errors given above. Although they are somewhat broad, the APDs of 16 Cyg A and B peak at nearly the same age. A much more precise age can be obtained by combining the two APDs, as shown with the solid line histogram in Fig. 5. This combined 16 Cyg APD is simply the product of the APDs of the components of the 16 Cyg binary system, normalized to 1 at the maximum. Using the combined APD we infer an age of $7.10^{+0.18}_{-0.35}$ Gyr for 16 Cyg. Note that this very small age error bar does not include systematic errors due to model uncertainties or errors introduced by statistical biases (see below). It represents only the internal precision of our method when applied to a binary system.

Stellar parameters derived from isochrones are subject to a number of systematic errors as well as statistical biases due to isochrone sampling which are described in detail by, for example, Nordström et al. (2004, their Sect. 4.5.4). Bayesian approaches have been proposed to tackle these problems (e.g., Pont & Eyer

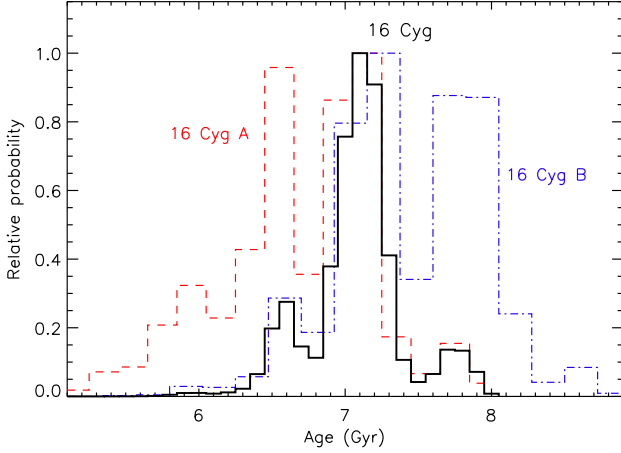


Figure 5. Normalized age probability distributions for 16 Cyg A (dashed histogram), 16 Cyg B (dot-dashed histogram), and the 16 Cyg binary system (solid line histogram).

2004; Jørgensen & Lindegren 2005; da Silva et al. 2006; Casagrande et al. 2011). We can compare our results with the Bayesian implementation by da Silva et al. (2006) since they provide a very convenient online tool that uses their method.¹³ We find $\log g(A) = 4.26 \pm 0.01$ and $\log g(B) = 4.31 \pm 0.01$, in excellent agreement with our estimates even though the choice of isochrones is different (da Silva et al. use PADOVA isochrones; e.g., Bertelli et al. 1994; Girardi et al. 2000) and we do not correct for statistical biases. The masses derived with the da Silva et al. (2006) online tool are about $0.02 M_{\odot}$ lower but the difference between 16 Cyg A and B is nearly identical. For the stellar ages, da Silva et al. online tool suggests 6.7 ± 0.5 Gyr (A) and 7.6 ± 0.7 Gyr (B). These values are also consistent with our derived age for the 16 Cyg system considering the 1σ uncertainties.

Note that the excitation/ionization method of atmospheric parameter determination was not able to resolve the small difference in $\log g$ found in this section although the results are also consistent within 1σ . Clearly, for nearby stars with well determined effective temperatures, parallaxes, and good photometry, the isochrone method is superior.

3.5. Surface gravity from the MgIb lines

The wings of certain strong spectral features are mildly sensitive to the stellar surface gravity. A particularly important feature in this regard is the MgIb triplet at about 5180 Å. The effective temperature and magnesium abundance must be known with high precision in order for this line to be useful in the determination of $\log g$.

Fig. 6 shows the spectral region around the strongest of the MgIb lines and the red wing of the middle one along with synthetic spectra computed for values of $\log g$ that reproduce best the regions free from lines other than the MgIb lines, such as those around 5174 Å and 5185 Å. We fine-tuned the transition probabilities of these lines to reproduce the solar MgIb lines with a Mg abundance of $A_{\text{Mg}} = 7.60$, as measured by Asplund et al. (2009). For 16 Cyg A and B we used synthetic models with our final T_{eff} and [Fe/H] values as well as our derived magnesium abundances. Synthetic profiles for $\log g \pm 0.2$ dex are also

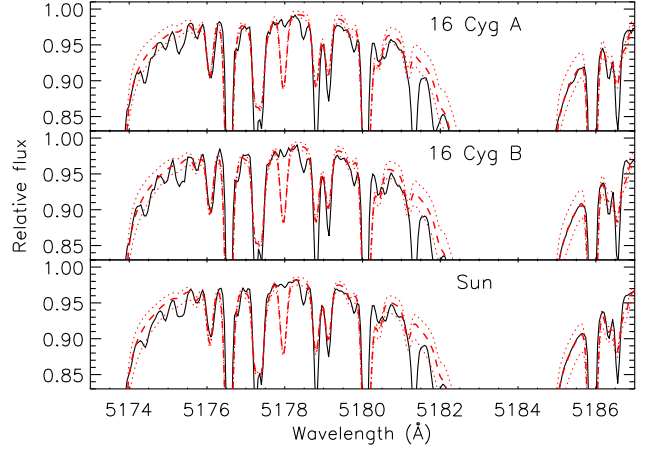


Figure 6. Spectral region showing the strongest of the MgIb lines and the red wing of the middle MgIb line in 16 Cyg A, 16 Cyg B, and the Sun. Dashed lines show best fit models for each star (with their derived $\log g$ values) while dotted lines correspond to synthetic spectra with $\log g \pm 0.2$.

Table 2
Effective temperature and surface gravity determinations

T_{eff} (K)	16 Cyg A	16 Cyg B
Fe lines	5818 ± 38	5742 ± 30
Colors (IRFM)	5792 ± 38	5733 ± 38
H α	5819 ± 25	5762 ± 26
Adopted	5813 ± 18	5749 ± 17
$\log g$ [cgs]	16 Cyg A	16 Cyg B
Fe lines	4.31 ± 0.05	4.31 ± 0.05
Trigonometric	4.28 ± 0.02	4.33 ± 0.02
MgIb	4.27 ± 0.04	4.33 ± 0.04
Adopted	4.282 ± 0.017	4.328 ± 0.017

Table 3
Basic data and derived parameters for the 16 Cyg binary system

	16 Cyg A	16 Cyg B
V (mag)	5.959 ± 0.009	6.228 ± 0.019
π (mas)	47.44 ± 0.27	47.14 ± 0.27
M_V (mag)	4.340 ± 0.015	4.595 ± 0.023
T_{eff} (K)	5813 ± 18	5749 ± 17
$\log g$ [cgs]	4.282 ± 0.017	4.328 ± 0.017
Mass (M_{\odot})	1.05 ± 0.02	1.00 ± 0.01

shown in Fig. 6 to illustrate the sensitivity of these features to $\log g$. From a least-squares minimization of the clean regions we find $\log g = 4.27 \pm 0.04$ for 16 Cyg A and $\log g = 4.33 \pm 0.04$ for 16 Cyg B, in excellent agreement with the values found in the previous section.

Similar to the case of T_{eff} , the three methods used to derive $\log g$ are independent so a weighted average can be used to determine the best solution. We find: $\log g(A) = 4.282 \pm 0.017$, $\log g(B) = 4.328 \pm 0.017$. These and other fundamental parameters derived in this section are summarized in Tables 2 and 3.

4. ELEMENTAL ABUNDANCES

Curve of growth analysis within MOOG was used to determine elemental abundances from equivalent width measurements of lines in the spectra of 16 Cyg A, B, and the Sun. We measured 288 lines for 22 elements; their

¹³ <http://stev.oapd.inaf.it/cgi-bin/param>

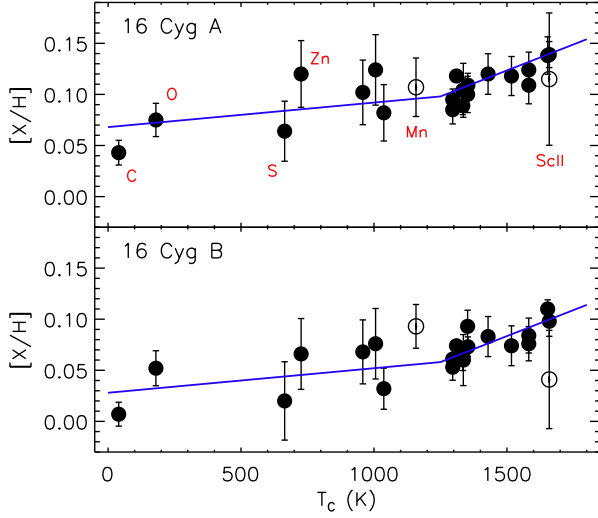


Figure 7. Elemental abundances of 16 Cyg A and B relative to our measured solar abundances as a function of dust condensation temperature for light elements ($Z \leq 30$). Solid lines show the mean trend of solar twin stars according to Meléndez et al. (2009) but shifted upwards in each case to match the mean abundance of volatile ($T_c < 900$ K) elements. Open circles correspond to Mn, Co, and Sc II.

EWs are given in Table 1. Since the oxygen abundances inferred from the infrared triplet lines, which are the only oxygen lines we use, are severely affected by non-LTE effects (e.g., Kiselman 1993; Fabbian et al. 2009), and reliable non-LTE computations can be found in the literature, we used the non-LTE correction tables by Ramírez et al. (2007) to take this systematic effect into account. Lines from two species (neutral and singly ionized) of Sc, Ti, Cr, and Fe were available; for the other elements only one species was measured. Good agreement was found for the abundances derived from two species of the same element except for Sc (see below). The abundances of Nd and Eu were determined using spectrum synthesis of a few carefully selected features. Spectrum synthesis was also employed to measure lithium abundances from the 6708 Å Li doublet.

We measured differential abundances on a line-by-line basis, which reduces the impact of errors in the atomic data and systematics in the modeling, given that these are all similar stars. Abundance ratios relative to solar ($[X/H]$) are listed in Table 4. Errors in this table correspond to the standard error of the line-to-line scatter added in quadrature with the random error introduced by the uncertainties in our derived atmospheric parameters. Fig. 7 shows the $[X/H]$ abundances as a function of the dust condensation temperature sequence by Lodders (2003) for the light elements ($Z \leq 30$). Heavy element ($Z > 30$) abundances are shown separately in Fig. 8. In both Figs. 7 and 8 we plot with a solid line the mean trend of solar twin stars by M09, shifted to match approximately the abundance pattern of $Z \leq 30$ elements for each star.

The weighted mean $[X/H]$ abundances from all species studied, which we denote by $[M/H]$, are $+0.103 \pm 0.023$ for 16 Cyg A and $+0.069 \pm 0.026$ for 16 Cyg B. The 16 Cyg binary system is therefore more metal-rich than the Sun but, interestingly, a small difference in the overall metal content appears to make 16 Cyg A more metal-rich than

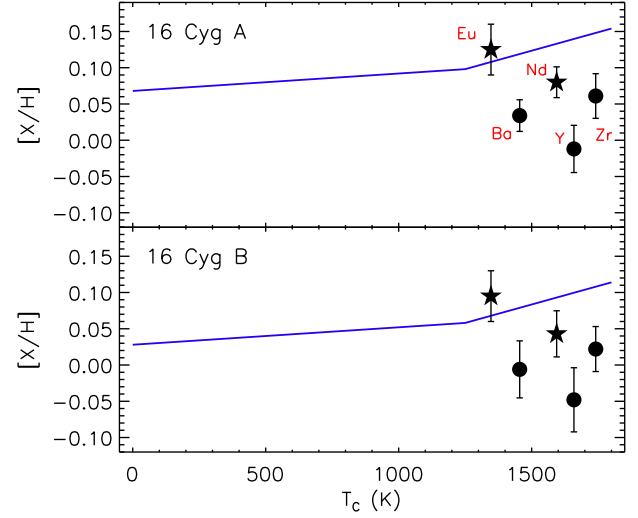


Figure 8. As in Fig. 7 for the heavy elements ($Z > 30$). Stars (circles) denote elemental abundances measured with spectrum synthesis (equivalent widths).

16 Cyg B.

Considering only the light elements ($Z \leq 30$, Fig. 7), the observed abundances of 16 Cyg A and B follow the typical pattern of solar twin stars, i.e., they correlate with dust condensation temperature as in M09. Note that the latter was obtained from the average abundances of 11 solar twin stars, resulting in a very small abundance error (of order 0.01 dex). However, for individual stars, the dispersion seen in Fig. 7 is fully consistent with the analysis by M09.

On the other hand, the heavy element abundances ($Z > 30$, Fig. 8) do not follow the typical solar twin behavior. Strictly speaking, 16 Cyg A and B are solar analogs and not solar twins, mainly due to their slightly lower surface gravities, which makes them more evolved than the Sun. Compared to the Sun, the 16 Cyg system is about 2.5 Gyr older and it is therefore likely that the anomalous abundances of the heavy elements (when compared to solar twins) are due to Galactic chemical evolution effects. We discuss these in detail in Sect. 5.2.

In principle, the mean metallicities ($[M/H]$) of 16 Cyg A and B are consistent within 1σ . We should point out, however, that this analysis uses our solar spectrum as reference. Although obtained with the same instrument, which is ideal, our solar spectrum was not observed in the exact same way the stellar spectra were taken. Important differences in the data reduction procedures are also present. Furthermore, our reference spectrum is based on observations of the daysky, which is known not to be an exact replica of the solar spectrum, although we attempted to minimize its impact by using daysky spectra at small angular distances from the Sun, as explained in Sect. 2.

Inspection of Figs. 7 and 8 shows clearly that the element to element scatter is very similar in 16 Cyg A and B. This suggests that the difference between A and B might be better established by comparing them directly rather than using our possibly faulty solar spectrum. Galactic chemical evolution effects will also be minimized, if not eliminated, with this approach. Thus, we measured differential abundances of 16 Cyg A, again on a line-by-

Table 4
Elemental abundances relative to solar ($[X/H]$) and differential between 16 Cyg A and B ($\Delta[X/H]$).

	Species	T_C (K)	$[X/H]$ (16 Cyg A)	error	$[X/H]$ (16 Cyg B)	error	$\Delta[X/H]$ (16 Cyg A–16 Cyg B)	error
6.0	C	40	0.043	0.012	0.007	0.012	0.037	0.016
8.0	O	180	0.075	0.016	0.052	0.018	0.024	0.024
11.0	Na	958	0.102	0.032	0.068	0.031	0.034	0.020
12.0	Mg	1336	0.104	0.026	0.060	0.026	0.043	0.013
13.0	Al	1653	0.138	0.018	0.110	0.018	0.028	0.023
14.0	Si	1310	0.118	0.006	0.074	0.004	0.044	0.008
16.0	S	664	0.064	0.029	0.020	0.030	0.044	0.016
19.0	K	1006	0.124	0.034	0.076	0.034	0.048	0.028
20.0	Ca	1517	0.118	0.019	0.074	0.018	0.044	0.017
21.0	ScI	1659	0.115	0.065	0.041	0.065	0.074	0.027
21.1	ScII	1659	0.139	0.013	0.098	0.012	0.041	0.011
22.0	TiI	1582	0.109	0.018	0.076	0.016	0.033	0.023
22.1	TiII	1582	0.124	0.017	0.084	0.017	0.040	0.009
23.0	V	1429	0.120	0.020	0.083	0.020	0.037	0.026
24.0	CrI	1296	0.085	0.014	0.053	0.013	0.033	0.018
24.1	CrII	1296	0.095	0.010	0.061	0.011	0.034	0.013
25.0	Mn	1158	0.107	0.029	0.093	0.028	0.014	0.022
26.0	FeI	1334	0.104	0.012	0.061	0.011	0.042	0.016
26.1	FeII	1334	0.089	0.009	0.064	0.010	0.025	0.013
27.0	Co	1352	0.100	0.018	0.093	0.016	0.007	0.018
28.0	Ni	1353	0.109	0.012	0.073	0.010	0.036	0.014
29.0	Cu	1037	0.082	0.028	0.032	0.028	0.051	0.019
30.0	Zn	726	0.120	0.033	0.066	0.033	0.053	0.008
39.1	Y	1659	-0.012	0.033	-0.048	0.044	0.036	0.016
40.1	Zr	1741	0.061	0.031	0.022	0.031	0.039	0.018
56.1	Ba	1455	0.034	0.022	-0.006	0.039	0.040	0.020
60.1	Nd	1594	0.080	0.021	0.043	0.032	0.030	0.035
63.1	Eu	1347	0.125	0.035	0.095	0.035	0.037	0.023

line basis, but using 16 Cyg B as the reference star. We denote these differential abundances with the symbol $\Delta[X/H]$. The results are given in Table 4. Similar to the errors in $[X/H]$, the errors listed in Table 4 for $\Delta[X/H]$ correspond to the standard error of the line-to-line scatter added in quadrature with the errors introduced by uncertainties in our derived stellar parameters. Fig. 9 shows the derived 16 Cyg A – 16 Cyg B relative abundances as a function of atomic number and dust condensation temperature. Note that in this case both the light and heavy elements behave similarly.

Fig. 9 shows that not only are the 1σ errors of the A–B relative abundances small but it also reveals that the element-to-element dispersion is extremely small. A weighted average of all species measured suggests a metallicity offset of $\Delta[M/H] = +0.040 \pm 0.010$ dex for 16 Cyg A relative to 16 Cyg B. The three species that depart the most from this average value are Sc I, Mn, and Co. It is tempting to attribute these discrepant data points to strong differential non-LTE effects (see Zhang et al. 2008 for Sc I, Bergemann & Gehren 2007 for Mn, and Bergemann 2008 for Co; see also Bergemann et al. 2010) since there is a difference of about 65 K in T_{eff} between the two stars in addition to a difference of 0.05 dex in $\log g$. Furthermore, we note that the Sc II abundance, which is known to be more reliable than Sc I, is consistent with the derived $\Delta[M/H]$ while the 1σ line-to-line scatter (not the standard error) of the Mn abundance difference is the largest of all species analyzed with equivalent widths. A more proper treatment of Co line formation requires consideration of hyperfine structure (HFS) splitting, which we tested for three Co I

features using HFS constants by Kurucz & Bell (1995). In this case we obtained $\Delta[\text{Co}/\text{H}] = +0.007 \pm 0.018$, in excellent agreement with the value derived from equivalent widths and ignoring HFS. Perhaps a combination of HFS and non-LTE effects could explain our Co abundances. Bergemann et al. (2010), for example, calculate a non-LTE correction of 0.13 dex for the Sun, which is relatively large. Excluding arbitrarily these three discrepant data points (Sc I, Mn, and Co), which are likely affected by small but non-negligible systematic errors in high precision work, the metallicity offset is: $\Delta[M/H] = +0.041 \pm 0.007$ (A–B). Hereafter, we discuss our results ignoring the Sc I, Mn, and Co abundances.

Note that the 1σ uncertainty of the metallicity difference that we inferred above corresponds to about 1 % on a linear scale. Interestingly, the 1σ error of our measured EW s is also about 1 %. This suggests that the error in our very precise elemental abundance determinations, which are based on curve of growth analysis (exclusively on the linear part) with the EW s as input data, is dominated by the observational errors (elements Nd and Eu are the only exceptions, since their abundances were measured using line profile fitting). Thus, it should be in principle possible to improve upon these estimates using even higher quality data.

We have explored the impact of systematic errors in our derived atmospheric parameters by arbitrarily modifying them and recomputing the abundances. First, we tried increasing and decreasing the T_{eff} values of both stars by 100 K. Interestingly, in both cases we find that the A–B metallicity difference decreases to about 0.03 dex but the element-to-element scatter increases to

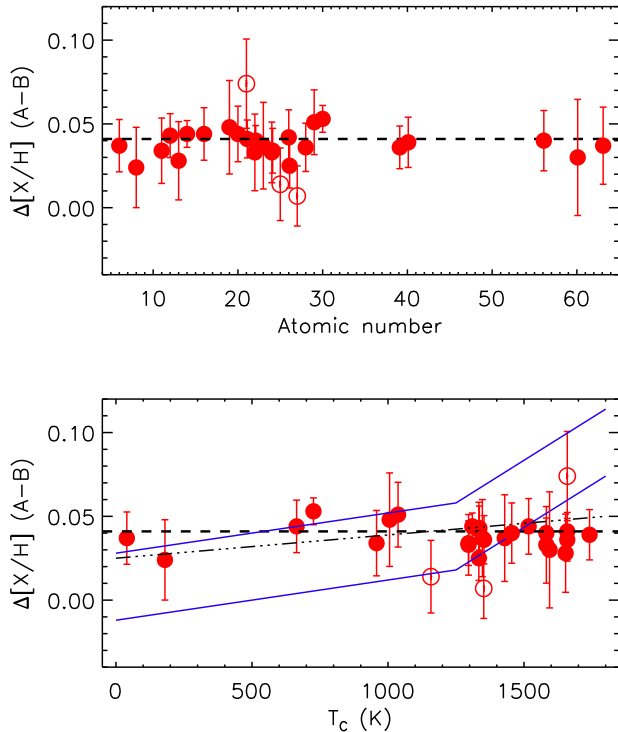


Figure 9. Top panel: elemental abundance difference between 16 Cyg A and B as a function of atomic number. Open symbols show the three species more discrepant from the mean: Sc (21), Mn (25), and Co (27). Bottom panel: as in the top panel for the abundance differences versus dust condensation temperature. The dashed line is at +0.041 while the solid lines represent the mean trend of solar twins by Meléndez et al. (2009) with two arbitrary offsets. The dot-dashed line corresponds to a slope of $1.4 \times 10^{-5} \text{ dex K}^{-1}$, as derived by Laws & Gonzalez (2001).

0.008 dex. Adopting identical $\log g = 4.30$ values for both stars increases the metallicity difference to +0.046 dex but in this case the element-to-element scatter increases significantly to 0.013 dex. The fact that the element-to-element scatter naturally minimizes for our derived parameters suggests that they are very reliable.

We have also re-determined our abundances using the differential parameters derived by Takeda (2005), who claims that there is no metallicity difference between 16 Cyg A and B. We kept our 16 Cyg B parameters fixed and adopted 16 Cyg A parameters consistent with Takeda’s. The inferred metallicity difference in this case is $+0.032 \pm 0.013$, i.e., we find that 16 Cyg A is still more metal-rich than 16 Cyg B. However, for these parameters we detect a small negative trend for the abundance differences and condensation temperature which makes the difference smaller for refractory elements like iron. For those elements the metallicity difference is about $+0.02 \pm 0.01$ dex. It seems possible that a combination of these effects is responsible for the Takeda (2005) results but we admit that we are unable to reproduce exactly his derived elemental abundances.

Our main result that 16 Cyg A is more metal-rich than 16 Cyg B was already suggested in the high precision work by Laws & Gonzalez (2001). They found, however, a metallicity difference of $+0.025 \pm 0.009$ based only on the analysis of iron lines. As a note added in proof they commented that abundances of 13 other ele-

ments were measured and showed a small positive correlation with dust condensation temperature. Their derived slope is shown in the bottom panel of our Fig. 9. Depending on the elements that one uses to calculate the slope, it could be possible to find good agreement between our data and the Laws & Gonzalez result. Nevertheless, using our abundances we obtain essentially a zero slope ($-0.2 \pm 0.6 \times 10^5 \text{ dex K}^{-1}$), which is inconsistent with the slope derived by Laws & Gonzalez ($+1.4 \pm 0.5 \times 10^5 \text{ dex K}^{-1}$). We argue that our results are more robust owing to the larger number of elements analyzed and the very high precision achieved for the overall metallicity difference.

Finally, using Kurucz’ model atmospheres we find $\Delta[M/H] = +0.039 \pm 0.007$ (no-overshoot models) and $\Delta[M/H] = +0.040 \pm 0.007$ (overshoot models). Thus, we demonstrate again that the choice of model atmosphere grid has an almost negligible impact on our results.

5. DISCUSSION

5.1. Planet signatures in stellar abundances

High precision elemental abundance work in solar twins and analogs has revealed a possible connection between the properties of a star and the process of planet formation that occurred around it. The work by M09 showed that, compared to the majority ($\simeq 85\%$) of solar twin stars, the Sun exhibits a deficiency of refractory elements relative to volatiles (of order 20%). They proposed that this solar abundance anomaly could be due to the formation of the terrestrial planets in the solar system since these objects are rich in refractory elements. Thus, the missing mass of refractory elements in the solar photosphere would be currently located in the terrestrial planets. This hypothesis assumes that the majority of solar twin stars did not form as many rocky objects as in the solar system or that if they did, they were accreted by the star at later times, possibly through orbital migration. Only about 15% of solar twin stars show a photospheric composition indistinguishable from the solar one. These objects are potentially terrestrial planet hosts. Later work by R09 and Ramírez et al. (2010) confirmed the observational results of M09 and expanded the sample towards higher metallicities, where they found that, based on the abundances measured, the fraction of terrestrial planet hosts increases towards higher $[\text{Fe}/\text{H}]$.

Thus, it seems likely that a “planet signature” has been imprinted in the chemical composition of the host stars and, arguably, it appears to relate only to the formation of rocky objects. Indeed, M09 showed that metal-rich solar analogs with giant planets detected have abundance patterns relative to iron similar to those of the majority of solar twins, suggesting that the solar abundance anomaly could not be related to the formation of the gas giants. This type of analysis, however, should be examined more carefully because the impact of systematic errors and Galactic chemical evolution could be important in this higher $[\text{Fe}/\text{H}]$ regime (see also Schuler et al. 2011). Data by independent groups have confirmed the observational result by M09 and R09 (Ramírez et al. 2010; González Hernández et al. 2010; Gonzalez et al. 2010b). Although the planet formation signature interpretation has been contended by González Hernández et al. (2010), a response to their criticism has been provided by

Ramírez et al. (2010). Alternative scenarios to explain the solar abundance anomaly have also been explored, without success (Ramírez et al. 2010; Meléndez et al. 2011; Kiselman et al. 2011).

The planet signature hypothesis described above has been quantitatively tested by Chambers (2010), who computed the effect of adding two Earth masses ($2M_{\oplus}$) of Earth-like material and $2M_{\oplus}$ of CM chondrite material to the present-day solar convective envelope. He finds that in this experiment the solar abundance anomaly would disappear, i.e., the Sun would not show the deficiency of refractory elements anymore. Thus, his calculations support the hypothesis that the missing mass of rock in the solar photosphere is currently locked-up in the rocky bodies of the solar system. A similar estimate has been recently made by Meléndez et al. (2011) who suggest an even larger amount of CM chondrite material ($4M_{\oplus}$). Although such large mass is not observed in the present-day asteroid belt, it has been suggested that small rocky bodies were very abundant when the Sun was formed, but most of the material from the asteroid belt was probably removed by strong resonances (e.g., Weidenschilling 1977; Chambers & Wetherill 2001; Petit et al. 2001).

Excluding the heavy elements (i.e., for $Z \leq 30$), the abundance patterns of both 16 Cyg A and 16 Cyg B are compatible with those observed in most solar twin stars (Fig. 7). Within the planet signature scenario, this implies that none of these objects host terrestrial planets or that any rocky body that once formed there has been accreted by the host star. Perhaps binary systems like 16 Cyg are not stable enough to retain any terrestrial planets that might form. The gas giant planet around 16 Cyg B is highly eccentric, a property that has been attributed by some authors to the influence of the stellar companion (e.g., Cochran et al. 1997; Mazeh et al. 1997). The lack of rocky planets around 16 Cyg B could also be related to the presence of the gas giant planet. As evidenced by the Kepler mission data, multiple systems with small planets rarely contain hot Jupiters (Latham et al. 2011). In any case, the abundances of 16 Cyg A and B are not unusual considering that only about 15% of solar twins share the exact same (solar) composition.

5.2. Impact of Galactic chemical evolution

The heavy elements clearly do not follow the typical solar twin trend (Fig. 8). With the exception of Eu, the other $Z > 30$ elements are found significantly below the mean solar twin trend. The Nd abundances are marginally consistent with the expected trend but the Y, Zr, and Ba abundances are irreconcilable with that pattern. These elements are produced primarily by neutron-capture reactions on timescales slow (the s -process) or rapid (the r -process) relative to the average β -decay rates of radioactive isotopes along the reaction chain. The s -process is associated with low- and intermediate-mass stars ($1.3 \lesssim M \lesssim 8.0 M_{\odot}$) on the asymptotic giant branch. The site (or sites) of the r -process is not known but is suspected to be associated with core collapse supernovae ($M \gtrsim 8.0 M_{\odot}$). These stellar timescales imply that r -process enrichment occurs earlier than s -process enrichment, which is confirmed by the observed heavy element abundance patterns in low metallicity stars in

the Galactic halo and disk (e.g., McWilliam 1997).

Each of the r - and s -process contribute about half of the elements with $Z > 30$ in the Sun, and, following pioneering work by Cameron (1973), the solar abundance of each isotope (or element) can be decomposed into r - and s -process fractions. For example, 72% of the solar Y was produced via the s -process (e.g., Simmerer et al. 2004). Similarly, 81% of Zr, 85% of Ba, 58% of Nd, and 3% of Eu in the Sun were produced by the s -process. These fractions represent the chemical inventory of one point in the Galactic interstellar medium 4.5 Gyr ago. The stars in the 16 Cyg system formed 2.5 Gyr earlier and they are slightly deficient in s -process material relative to the Sun. As can be seen in Fig. 8, elements with a significant s -process component, such as Y, Zr, and Ba, are the most deficient. Nd, which has roughly equal contributions from the r - and s -processes, is moderately deficient, and Eu, which has a minimal s -process contribution, is not deficient at all. The fact that the heavy elements in both 16 Cyg A and B show the same abundance pattern as a function of T_{C} suggests that this is a primordial effect—the result of Galactic chemical evolution (GCE). The slightly super-solar metallicity of the system is not in contradiction, as the slope of $[\text{Ba}/\text{H}]$ versus time is steeper than that for $[\text{Fe}/\text{H}]$ (e.g., Edvardsson et al. 1993).

The works by M09 and R09 concentrated only on solar twin stars, therefore minimizing these relatively small GCE effects. Nevertheless, it is interesting to note that the solar twin abundances of Y, Zr, and Ba by R09 show larger star-to-star error than those of lighter elements (see their Figs. 1 and 3), a result that could be associated to the age span of their sample. The opposite effect of that observed in the 16 Cyg system (i.e., neutron capture element abundances higher than the mean solar twin trend) has been recently observed in the younger solar twin star 18 Sco (Meléndez et al., in preparation), reinforcing the idea that this is related to GCE. Thus, our results for the heavy elements tell us that extreme caution must be practiced when interpretations of abundance ratios versus condensation temperature are made for stars that are not so similar to the Sun, in particular stars that are significantly older or younger, because GCE effects are not entirely negligible.

5.3. Did 16 Cyg A accrete planetary material? Clues from lithium abundances

Based on the discussion given in the previous sections, we are led to conclude that the metallicity difference between 16 Cyg A and B is not primordial but acquired. Either the photosphere of 16 Cyg A became more metal-rich or that of 16 Cyg B became more metal-poor after they were formed (or while they were being formed) from the same molecular cloud with the same initial chemical composition. Laws & Gonzalez (2001) suggested that 16 Cyg A accreted either 2.5 Earth masses of chondritic material or $0.3 M_{\text{J}}$ of gas giant material to explain its higher $[\text{Fe}/\text{H}]$ (they derived $\Delta[\text{Fe}/\text{H}] = +0.025 \pm 0.009$). They also argued that the late accretion of planetary material could increase the lithium abundance on the star's convective envelope. Indeed, inspection of the 6708 Å region clearly shows that 16 Cyg B is lithium poor compared to 16 Cyg A (Fig. 10). Our derived Li abundances are: $A(\text{Li}) = 1.34 \pm 0.04$ for 16 Cyg A and

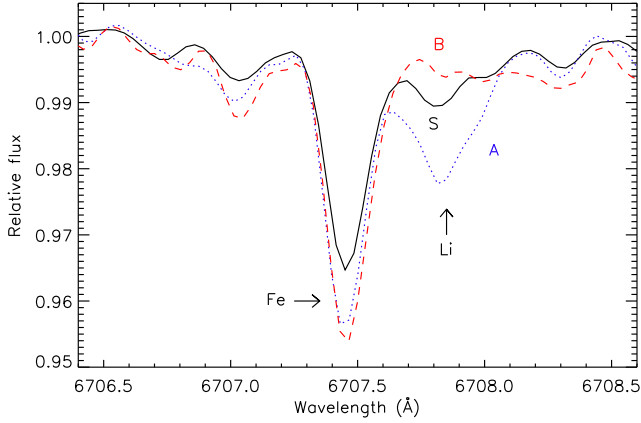


Figure 10. Spectral region around the Li doublet feature (6708 Å). Our solar spectrum (solid line) is shown along spectra of 16 Cyg A (dotted line) and 16 Cyg B (dashed line).

$A(\text{Li}) = 0.73 \pm 0.06$ for 16 Cyg B, in good agreement with previously published estimates (King et al. 1997; Luck & Heiter 2006; Takeda et al. 2007; Israelian et al. 2009; Baumann et al. 2010). Thus, 16 Cyg A has about 4.1 times ($\simeq 0.6$ dex) more lithium than 16 Cyg B in its photosphere.

The behavior of Li abundances in solar-type stars is very complex and not yet fully understood (e.g., Chaboyer 1998; Pinsonneault 2010). In general, however, inspection of large samples clearly shows that at around $1 M_{\odot}$ and $T_{\text{eff}} = 5780 \text{ K}$ a very steep slope of increasing Li abundances with stellar mass (or T_{eff}) is present (e.g., Takeda et al. 2007; Baumann et al. 2010). Fitting a straight line to the Li abundance versus T_{eff} relation of stars in the 5700–5900 K range we find that the lithium abundances of stars with T_{eff} values similar to those of 16 Cyg A and B should differ by a factor of 3.5 ($\simeq 0.55$ dex), i.e., very close to the observed value. Fish et al. (in preparation) have recently derived lithium abundances of more than 700 solar-type stars and compiled and homogenized lithium abundance data for more than 1400 FGK stars. They also derive masses and ages in a consistent manner employing the exact same method used in this work. The lithium versus age trends for stars of mass and metallicity similar to those of 16 Cyg A and B, taken from the Fish et al. catalog, are shown in Fig. 11. The lithium abundances of both 16 Cyg A and B are perfectly normal for stars of their mass, age, and metallicity, despite the somewhat large scatter, in particular for stars like 16 Cyg B.

If the convective envelope of 16 Cyg A, after it reached its present size, accreted $0.3 M_{\text{J}}$ of planetary material that has not experienced lithium depletion, as suggested by Laws & Gonzalez (2001), the photospheric lithium abundance would have increased by about 0.4 dex (a factor of 2.5). Thus, if 16 Cyg A was polluted by planetary material, considering the mass effect on lithium depletion, the lithium abundance of 16 Cyg A should be about one order of magnitude larger than that of 16 Cyg B, which is significantly larger than observed. Such large lithium abundance for 16 Cyg A would also make the star somewhat lithium rich compared to stars of similar mass and metallicity (top panel in Fig. 11). Already the mass effect explains most, if not all, of the observed difference.

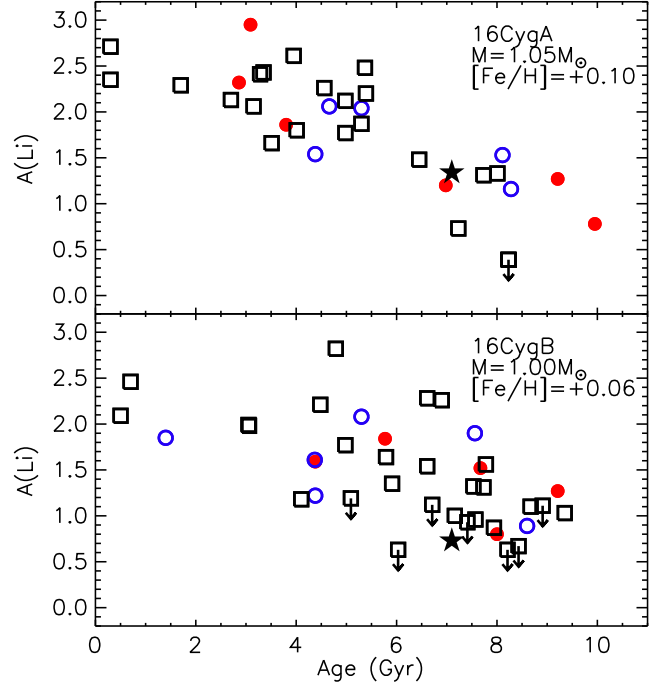


Figure 11. Evolution of lithium abundance for stars of mass and metallicity similar to those of 16 Cyg A (top panel) and 16 Cyg B (bottom panel). In each panel the stellar mass is within $0.03 M_{\odot}$ and metallicity within 0.05 dex from those of the 16 Cyg stars. Only stars with age/error > 3 are plotted. Upper limits on Li abundances are shown with downwards arrows. Open (filled) circles represent stars without (with) gas giant planets detected while open squares correspond to stars for which planet information is not available. Five-pointed stars show the location of 16 Cyg A (top panel) and 16 Cyg B (bottom panel).

The work by Deliyannis et al. (2000) on beryllium abundances also provides no evidence for accretion of planetary material by 16 Cyg A, although the authors warn that the errors are too large to make a firm conclusion.

5.4. A signature of gas giant planet formation?

A different possibility to explain the elemental abundance differences in the 16 Cyg system is that it was produced by the formation of the planet around 16 Cyg B. Similar to M09, we propose that the convective zone of 16 Cyg B has been depleted of metals due to the formation of a planet, i.e., that the missing mass of metals in 16 Cyg B is currently locked-up in its planet.

Before exploring this hypothesis in detail, we should re-address the problem of lithium abundance. A number of authors have suggested that lower lithium abundances could be correlated with the presence of gas giants (e.g., Israelian et al. 2009; Gonzalez et al. 2010a), although their preferred explanation is that it relates to physical processes that affect the rotational evolution of stars with planets and hence their lithium depletion history. A few planet-hosts and single stars are plotted in Fig. 11. Age, mass, and metallicity effects fully explain the observed abundances of both types of stars, without invoking the presence or absence of gas giant planets, consistent with the works by, for example, Baumann et al. (2010) and Ghezzi et al. (2010). This is the case also for the 16 Cyg stars; i.e., the significantly lower lithium abundance of 16 Cyg B ($\simeq 0.6$ dex relative to 16 Cyg A) is not due to the presence of its planet. In

our hypothesis, however, a very small fraction of this difference (≈ 0.04 dex) could be due to the formation of the gas giant planet around 16 Cyg B. However, the effect is not related to enhanced lithium depletion in the photosphere of 16 Cyg B but to the fact that the planet around 16 Cyg B retained a certain amount of lithium that would have otherwise been accreted by the star.

As shown in Fig. 9, the 16 Cyg A–B abundance differences do not correlate with dust condensation temperature as in M09. If we force the volatiles to match the mean abundance pattern of solar twins, the refractories are too low by 0.06 dex and vice-versa (see solid lines in Fig. 9). If the metallicity difference between 16 Cyg A and B is due to the formation of the planet around 16 Cyg B, we must assume that the abundance ratios of metals in this planet are very similar to those in the star 16 Cyg B. In particular, we have to assume that the volatile to refractory abundance ratios are equal to those in the photosphere of 16 Cyg B (excluding H and He, of course). Thus, the planet must be a gas giant, as indeed observed.

We explore our hypothesis quantitatively with a toy model. If the planet around 16 Cyg B were to be added to the convective zone of the star, the stellar metallicity would change by:

$$\Delta[\text{M}/\text{H}] = \log \left[\frac{(Z/X)_{\text{CZ}} M_{\text{CZ}} + (Z/X)_{\text{p}} M_{\text{p}}}{(Z/X)_{\text{CZ}} M_{\text{CZ}}} \right], \quad (1)$$

where $(Z/X)_{\text{CZ}}$ is the ratio of the fractional abundance of metals (Z) relative to hydrogen (X) in the unperturbed convective zone (loosely called “metallicity” in this context), M_{CZ} the mass of the convective zone, $(Z/X)_{\text{p}}$ the metallicity of the planet, and M_{p} the mass of the planet. According to Asplund et al. (2009), $(Z/X)_{\text{CZ}}^{\odot} = 0.018$. Thus, for 16 Cyg B ($[\text{M}/\text{H}] = 0.061$) we adopt $(Z/X)_{\text{CZ}} = 10^{0.061} \times 0.018 = 0.021$.

We can use Eq. 1 to calculate the mass of the convective envelope necessary to explain the observed metallicity difference of $\Delta[\text{M}/\text{H}] = +0.04$ given the planetary parameters $(Z/X)_{\text{p}}$ and M_{p} . Since a minimum mass estimate of $1.5 M_{\text{J}}$ is available from the work by Cochran et al. (1997), we explore Eq. 1 for a range of planet masses from 1.5 to $9.5 M_{\text{J}}$. The results from our toy model are illustrated in Fig. 12.¹⁴

This toy model is intended to counteract the immediate aftermath of the planet formation process. Thus, the mass of the convective envelope that appears in Eq. 1 corresponds to the convective zone at the time of planet formation. Standard models of early stellar evolution suggest that solar analog stars begin fully convective and only after about 30 Myr their convective envelopes reach their present-day masses (e.g., D’Antona & Mazzitelli 1994; Serenelli et al. 2011). On the other hand, observations of disks around young stars suggest a shorter timescale for the process of planet formation, of order 10 Myr (e.g., Mamajek 2009; Meyer 2009; Fedele et al.

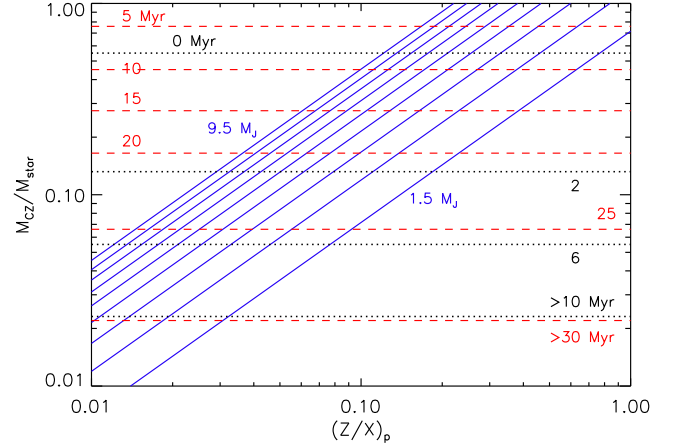


Figure 12. Solid lines correspond to the mass of the convective envelope of 16 Cyg B necessary to explain the metallicity difference between 16 Cyg A and B as a function of the metallicity of the planet around 16 Cyg B and for planet masses between 1.5 and $9.5 M_{\text{J}}$ in increments of $1.0 M_{\text{J}}$. Dashed lines correspond to the mass of the convective envelope of 16 Cyg B for stellar ages between 5 and > 30 Myr according to the standard model by Serenelli et al. (2011). Dotted lines represent a similar evolution for M_{CZ} , from 0 to 10 Myr, but according to one of the non-standard models with episodic accretion by Baraffe & Chabrier (2010).

2010). Thus, we investigate our simple model keeping M_{CZ} as a variable quantity but constraining its temporal evolution as computed by Serenelli et al. (2011, their Fig. 1). The latter corresponds to a $1 M_{\odot}$ star of solar-metallicity. To take into account the small differences in mass and $[\text{Fe}/\text{H}]$ for 16 Cyg B, we scaled the Serenelli et al. (2011) result using the present-day convective envelope masses as a function of T_{eff} , $[\text{Fe}/\text{H}]$ by Pinsonneault et al. (2001). The dashed lines plotted in Fig. 12 correspond to the mass of the convective zone at different stellar ages according to standard models. In this figure we also show, with dotted lines, the time evolution of M_{CZ} for one of the non-standard models with episodic accretion by Baraffe & Chabrier (2010). We discuss this case later in this section.

According to our pollution model with standard M_{CZ} evolution, if the planet has $(Z/X)_{\text{p}} = 0.1$ and $M_{\text{p}} = 1.5 M_{\text{J}}$, it should have formed when the star was about 25 Myr old but if the planet has $M_{\text{p}} = 9.5 M_{\text{J}}$, it should have formed 10 Myr after the star was born, when the convective envelope was more massive, therefore diluting more the larger amount of metal-depleted gas accreted. The planet around 16 Cyg B could not have formed 25 Myr after the stellar birth since the convective envelope at that point was too small. Only if the metallicity of the planet is significantly lower (< 0.03) it could have formed at these late times. On the other hand, if the planet is more metal rich, for example $(Z/X)_{\text{p}} = 0.7$, it must have formed in the first 10 Myr since the birth of the star, and earlier for larger planet masses. Such large planet metallicity appears, however, unphysical for gas giants. The amount of metals in Jupiter (core and envelope) is about $12\text{--}37 M_{\oplus}$ (Guillot 2005; Fortney & Nettelmann 2010) and it seems that all giant planets have at least $10\text{--}15 M_{\oplus}$ of metals (Miller & Fortney 2011). Since Jupiter’s mass is $318 M_{\oplus}$, a total amount of metals of $12\text{--}37 M_{\oplus}$ would imply $(Z/X)_{\text{p}} = 0.04\text{--}0.12$.

Theoretical models of planet formation predict that

¹⁴ Our simple model assumes instantaneous accretion of metal-deficient material, therefore implying that the planet itself formed instantaneously, which is a very crude approximation. More detailed models should consider the finite formation time scale of the planet in addition to the temporal evolution of the mass of the convective envelope but that is beyond the scope of our work. Our results are therefore only useful as first order approximations.

gas giant planets form relatively quickly, on time scales shorter than 10 Myr (e.g., Pollack et al. 1996; Guilera et al. 2011). Yet, for reasonable values of the planet’s metallicity and mass, planet formation time scales from our pollution model with standard M_{CZ} evolution are in the 10–30 Myr range, i.e., we require the process of gas giant planet formation to be significantly longer. The exact same problem is faced by M09 scenario for the formation of terrestrial planets. They have to assume that while the terrestrial planets were being formed, the mass of the solar convective envelope had already reached its present size. A possible solution to this problem may lie in the new developments in the field of early stellar evolution. In particular, the impact of episodic accretion on the internal structure of stars may help solving this discrepancy.

Models for the early evolution of stars with non-steady accretion have been computed by Baraffe & Chabrier (2010). They demonstrate that the internal evolution of stars is highly dependent on the accretion history. Of particular interest for our work is the fact that their accretion models predict higher central temperatures and hotter overall structures leading to a more rapid formation of the radiative core in solar-type stars. In one of their models, the mass of the convective envelope of a $1 M_{\odot}$ star reaches its present-day size after only about 10 Myr from the stellar birthline. The evolution of M_{CZ} for this model in particular is represented with the dotted lines in Fig. 12.

One possibility to explain the metallicity difference between 16 Cyg A and B in the context of gas giant planet formation, and at the same time remain compatible with the terrestrial planet signature hypothesis by M09, consists in assuming that the gas giants formed during the first $\simeq 5$ Myr after the birth of the star whereas the terrestrial planets formed later ($\gtrsim 10$ Myr). More specifically, the timescales of accretion of metal-deficient and fractionated gas should be consistent with this assumption. In addition, the evolution of M_{CZ} should be quicker than predicted by standard models; i.e., M_{CZ} should reach its present day mass in about 10 Myr, as it is the case of some of the Baraffe & Chabrier (2010) models.

5.5. Elemental abundances in the solar nebula

An interesting consequence of the proposed scenario is that the solar nebula would have been more metal-rich than the present-day solar photosphere. In fact, we could re-construct the original solar abundances if we had a good knowledge of the composition of the gas giants. The combined mass of the gas giants in the solar system is about $1.4 M_J$, slightly lower than the minimum mass of the planet around 16 Cyg B. On the other hand, the convective envelope of the Sun is somewhat less massive than that of 16 Cyg B. Given the uncertainties in the many parameters involved to calculate the metallicity shift due to the formation of the gas giants in the solar system, we will assume for simplicity that their impact was similar to the case of 16 Cyg B. Thus, the formation of the gas giants in the solar system could have shifted the solar abundances of all elements down by about 0.04 dex. Later, the formation of rocky planets lowered even more the abundances of refractory elements by up to 0.08 dex while keeping the volatile abundances nearly constant (cf. M09, R09). Thus, for example, the abundances

of some important elements in the solar nebula would have been $[C, N, O/H] \simeq +0.05$, $[Fe/H] \simeq +0.09$, and $[Al, Sc, Ti/H] \simeq 0.12$. Note that in this calculation we have ignored the impact of diffusion, which would further decrease the present-day observed solar abundances by about 0.05 dex (Turcotte & Wimmer-Schweingruber 2002). Naturally, if the mass of the planet around 16 Cyg B is significantly larger than $1.5 M_J$, the impact of the formation of Jupiter on the solar abundances would be lower than 0.04 dex.

The elemental abundances measured in CM chondrite meteorites, which are often assumed to have retained the solar nebula composition, agree very well with those measured in the present-day solar photosphere (e.g., Lodders 2003; Asplund et al. 2009). The impact of planet formation and diffusion on the solar abundances described above is not necessarily in contradiction with this observation because when these comparisons are made the meteoritic abundances have to be normalized using the solar abundance of Si (or a mixture of several metals with low abundance uncertainties), therefore removing any overall metallicity offsets. The trend with condensation temperature, however, would not disappear in this way but it has not yet been detected, probably owing to the still relatively large errors in the determination of absolute solar elemental abundances.

According to our proposed scenario, the differences between the initial and present-day solar abundances are not negligible and they could be relevant for example in studies of Galactic chemical evolution, chemical tagging of dynamical groups, and stellar interior modeling. Further work on the impact of planet formation on stellar abundances, both from the observational and theoretical sides, is therefore urgently needed.

6. SUMMARY

We have determined the stellar parameters and abundances of 25 elements in 16 Cyg A and 16 Cyg B with very high precision. Their lithium abundances appear perfectly normal considering the observed lithium depletion patterns in field solar-type stars as a function of mass and metallicity and the small (but non-negligible) differences in these two parameters for the 16 Cyg stars. Accretion of planetary material onto 16 Cyg A and enhanced photospheric lithium depletion due to the presence of the planet around 16 Cyg B are not necessary to explain the observed lithium abundances.

Excluding lithium, we show that 16 Cyg A is more metal-rich than 16 Cyg B by $\Delta[M/H] = +0.041 \pm 0.007$ dex. The abundance differences detected do not correlate with dust condensation temperature. Thus, if the difference is due to the accretion of metal-depleted gas onto 16 Cyg B, the abundance ratios of different metals in this gas, in particular the volatile to refractory abundance ratio, should be nearly the same as that found today in the photosphere of 16 Cyg B. We propose a scenario in which both 16 Cyg A and B started with the exact same composition but the formation of a planet around 16 Cyg B made this secondary star slightly metal-poor. The composition of the planet must be the same as that of the stars (with the exception of H and He) in order for this hypothesis to work on a quantitative basis. Moreover, the planet must have formed while the convective envelope of the star was still relatively massive

(about 10% of the stellar mass).

The idea proposed to explain the abundance differences in the 16 Cyg binary system is similar to that suggested by Meléndez et al. (2009) and Ramírez et al. (2009) to explain the anomalous solar abundances as a signature of the formation of terrestrial planets. The main difference is that the planet around 16 Cyg B is a gas giant. We can reconcile these two hypothesis by assuming that gas giants form while the convective envelope is massive whereas terrestrial planets form later, when the convective zone reaches its present-day size. In any case, the formation of the stellar radiative core should be quicker than that predicted by standard stellar evolution models. The impact of episodic accretion on early stellar evolution could provide a solution to this problem.

If this scenario is correct, we must conclude that the Sun's original metallicity was higher, an effect possibly enhanced by atomic diffusion. Perhaps the regions immediately below the base of the solar convective envelope are significantly more metal-rich than the photosphere, a condition that has been proposed as a possible solution to the so-called solar abundance crisis (e.g., Nordlund 2009), i.e., the severe discrepancy between the observed photospheric solar abundances and those inferred from helioseismological data and stellar interior models (e.g., Basu & Antia 2004, 2008; Bahcall et al. 2005; Delahaye & Pinsonneault 2006). Note, however, that this idea seems not to work very well on a detailed, quantitative basis (e.g., Serenelli et al. 2011).

Our detail study of the 16 Cyg system shows that high precision elemental abundance work in wide binary stars with planets can provide us with important clues to understand the impact of planet formation on the chemical composition of stars. We encourage future spectroscopic studies of binary stars with similar components, both to measure small differences in their chemical composition and to look for planets, especially if the stars are solar analogs.

I.R.'s work was performed under contract with the California Institute of Technology (Caltech) funded by NASA through the Sagan Fellowship Program. J.M. would like to acknowledge support from FAPESP (2010/17510-3). I.U.R. is supported by the Carnegie Institution of Washington through the Carnegie Observatories Fellowship. We thank P. Barklem for computing the fine grid of theoretical $H\alpha$ profiles used to measure T_{eff} . I.R. would also like to thank D. L. Lambert, D. R. Doss, and the McDonald Observatory staff for observing support.

REFERENCES

- Allende Prieto, C., Barklem, P. S., Lambert, D. L., & Cunha, K. 2004, *A&A*, 420, 183
- Asplund, M., Grevesse, N., Sauval, A. J., & Scott, P. 2009, *ARA&A*, 47, 481
- Bahcall, J. N., Basu, S., Pinsonneault, M., & Serenelli, A. M. 2005, *ApJ*, 618, 1049
- Baraffe, I., & Chabrier, G. 2010, *A&A*, 521, A44
- Barklem, P. S., & Asplund-Johansson, J. 2005, *A&A*, 435, 373
- Barklem, P. S., Piskunov, N., & O'Mara, B. J. 2000, *A&AS*, 142, 467
- Barklem, P. S., Stempels, H. C., Allende Prieto, C., Kochukhov, O. P., Piskunov, N., & O'Mara, B. J. 2002, *A&A*, 385, 951
- Basu, S., & Antia, H. M. 2004, *ApJ*, 606, L85
- . 2008, *Phys. Rep.*, 457, 217
- Baumann, P., Ramírez, I., Meléndez, J., Asplund, M., & Lind, K. 2010, *A&A*, in press
- Bensby, T., Feltzing, S., Lundström, I., & Ilyin, I. 2005, *A&A*, 433, 185
- Bergemann, M. 2008, *Physica Scripta Volume T*, 133, 014013
- Bergemann, M., & Gehren, T. 2007, *A&A*, 473, 291
- Bergemann, M., Pickering, J. C., & Gehren, T. 2010, *MNRAS*, 401, 1334
- Bertelli, G., Bressan, A., Chiosi, C., Fagotto, F., & Nasi, E. 1994, *A&AS*, 106, 275
- Cameron, A. G. W. 1973, *Space Sci. Rev.*, 15, 121
- Casagrande, L., Ramírez, I., Meléndez, J., Bessell, M., & Asplund, M. 2010, *A&A*, 512, 54
- Casagrande, L., Schönrich, R., Asplund, M., Cassisi, S., Ramírez, I., Meléndez, J., Bensby, T., & Feltzing, S. 2011, *A&A*, 530, A138
- Chaboyer, B. 1998, in *IAU Symposium*, Vol. 185, *New Eyes to See Inside the Sun and Stars*, ed. F.-L. Deubner, J. Christensen-Dalsgaard, & D. Kurtz, 25
- Chambers, J. E. 2010, *ApJ*, 724, 92
- Chambers, J. E., & Wetherill, G. W. 2001, *Meteoritics and Planetary Science*, 36, 381
- Cochran, W. D., Hatzes, A. P., Butler, R. P., & Marcy, G. W. 1997, *ApJ*, 483, 457
- da Silva, L., et al. 2006, *A&A*, 458, 609
- D'Antona, F., & Mazzitelli, I. 1994, *ApJS*, 90, 467
- Delahaye, F., & Pinsonneault, M. H. 2006, *ApJ*, 649, 529
- Deliyannis, C. P., Cunha, K., King, J. R., & Boesgaard, A. M. 2000, *AJ*, 119, 2437
- Den Hartog, E. A., Lawler, J. E., Sneden, C., & Cowan, J. J. 2003, *ApJS*, 148, 543
- Desidera, S., Gratton, R. G., Lucatello, S., & Claudi, R. U. 2006, *A&A*, 454, 581
- Desidera, S., et al. 2004, *A&A*, 420, 683
- Edvardsson, B., Andersen, J., Gustafsson, B., Lambert, D. L., Nissen, P. E., & Tomkin, J. 1993, *A&A*, 275, 101
- Fabbian, D., Asplund, M., Barklem, P. S., Carlsson, M., & Kiselman, D. 2009, *A&A*, 500, 1221
- Fedele, D., van den Ancker, M. E., Henning, T., Jayawardhana, R., & Oliveira, J. M. 2010, *A&A*, 510, 72
- Fish, J. R., Ramírez, I., & et al. 2011, in preparation
- Fortney, J. J., & Nettelmann, N. 2010, *Space Sci. Rev.*, 152, 423
- Friel, E., Cayrel de Strobel, G., Chmielewski, Y., Spite, M., Lebre, A., & Bentolila, C. 1993, *A&A*, 274, 825
- Fuhrmann, K., Axer, M., & Gehren, T. 1994, *A&A*, 285, 585
- Ghezzi, L., Cunha, K., Smith, V. V., & de la Reza, R. 2010, *ApJ*, 724, 154
- Girardi, L., Bressan, A., Bertelli, G., & Chiosi, C. 2000, *A&AS*, 141, 371
- Gonzalez, G., Carlson, M. K., & Tobin, R. W. 2010a, *MNRAS*, 403, 1368
- . 2010b, *MNRAS*, 407, 314
- González Hernández, J. I., Israelian, G., Santos, N. C., Sousa, S., Delgado Mena, E., Neves, V., & Udry, S. 2010, *ApJ*, 720, 1592
- Gratton, R. G., Bonanno, G., Claudi, R. U., Cosentino, R., Desidera, S., Lucatello, S., & Scuderi, S. 2001, *A&A*, 377, 123
- Gray, D. F. 1992, *The observation and analysis of stellar photospheres* (Cambridge ; New York : Cambridge University Press, 1992. 2nd ed.)
- Gray, D. F., Tycner, C., & Brown, K. 2000, *PASP*, 112, 328
- Guilera, O. M., Fortier, A., Brunini, A., & Benvenuto, O. G. 2011, *ArXiv e-prints*
- Guillot, T. 2005, *Annual Review of Earth and Planetary Sciences*, 33, 493
- Gustafsson, B., Edvardsson, B., Eriksson, K., Jørgensen, U. G., Nordlund, Å., & Plez, B. 2008, *A&A*, 486, 951
- Hauser, H. M., & Marcy, G. W. 1999, *PASP*, 111, 321
- Hubeny, I. 1988, *Computer Phys. Comm.*, 52, 103
- Hubeny, I., & Lanz, T. 1995, *ApJ*, 439, 875
- Israelian, G., et al. 2009, *Nature*, 462, 189
- Ivans, I. I., Simmerer, J., Sneden, C., Lawler, J. E., Cowan, J. J., Gallino, R., & Bisterzo, S. 2006, *ApJ*, 645, 613
- Johnson, J. A., Aller, K. M., Howard, A. W., & Crepp, J. R. 2010, *PASP*, 122, 905
- Jørgensen, B. R., & Lindegren, L. 2005, *A&A*, 436, 127

- Kim, Y., Demarque, P., Yi, S. K., & Alexander, D. R. 2002, *ApJS*, 143, 499
- King, J. R., Deliyannis, C. P., Hiltgen, D. D., Stephens, A., Cunha, K., & Boesgaard, A. M. 1997, *AJ*, 113, 1871
- Kiselman, D. 1993, *A&A*, 275, 269
- Kiselman, D., Pereira, T., Gustafsson, B., & et al. 2011, *A&A*, submitted
- Kurucz, R., & Bell, B. 1995, *Atomic Line Data* (R.L. Kurucz and B. Bell) Kurucz CD-ROM No. 23. Cambridge, Mass.: Smithsonian Astrophysical Observatory, 1995., 23
- Latham, D. W., et al. 2011, *ApJ*, 732, L24+
- Lawler, J. E., Wickliffe, M. E., den Hartog, E. A., & Sneden, C. 2001, *ApJ*, 563, 1075
- Laws, C., & Gonzalez, G. 2001, *ApJ*, 553, 405
- Lodders, K. 2003, *ApJ*, 591, 1220
- Luck, R. E., & Heiter, U. 2006, *AJ*, 131, 3069
- Mamajek, E. E. 2009, in *American Institute of Physics Conference Series*, Vol. 1158, American Institute of Physics
- Conference Series, ed. T. Usuda, M. Tamura, & M. Ishii, 3–10
- Marcy, G., Butler, R. P., Fischer, D., Vogt, S., Wright, J. T., Tinney, C. G., & Jones, H. R. A. 2005, *Progress of Theoretical Physics Supplement*, 158, 24
- Mazeh, T., Krymolowski, Y., & Rosenfeld, G. 1997, *ApJ*, 477, L103
- McWilliam, A. 1997, *ARA&A*, 35, 503
- Meléndez, J., Asplund, M., Gustafsson, B., & Yong, D. 2009, *ApJ*, 704, L66
- Meléndez, J., Bergemann, M., Cohen, J. G., & et al. 2011, *A&A*, submitted
- Meléndez, J., & Ramírez, I. 2007, *ApJ*, 669, L89
- Mermilliod, J., Mermilliod, M., & Hauck, B. 1997, *A&AS*, 124, 349
- Meyer, M. R. 2009, in *IAU Symposium*, Vol. 258, IAU Symposium, ed. E. E. Mamajek, D. R. Soderblom, & R. F. G. Wyse, 111–122
- Miller, N., & Fortney, J. J. 2011, *ArXiv e-prints*
- Neves, V., Santos, N. C., Sousa, S. G., Correia, A. C. M., & Israelian, G. 2009, *A&A*, 497, 563
- Nordlund, A. 2009, *ArXiv e-prints*
- Nordström, B., et al. 2004, *A&A*, 418, 989
- Patience, J., et al. 2002, *ApJ*, 581, 654
- Perryman, M. A. C., et al. 1997, *A&A*, 323, L49
- Petit, J.-M., Morbidelli, A., & Chambers, J. 2001, *Icarus*, 153, 338
- Pinsonneault, M. H. 2010, in *IAU Symposium*, Vol. 268, IAU Symposium, ed. C. Charbonnel, M. Tosi, F. Primas, & C. Chiappini, 375–380
- Pinsonneault, M. H., DePoy, D. L., & Coffee, M. 2001, *ApJ*, 556, L59
- Pollack, J. B., Hubickyj, O., Bodenheimer, P., Lissauer, J. J., Podolak, M., & Greenzweig, Y. 1996, *Icarus*, 124, 62
- Pont, F., & Eyer, L. 2004, *MNRAS*, 351, 487
- Porto de Mello, G. F., & da Silva, L. 1997, *ApJ*, 482, L89
- Ramírez, I., Allende Prieto, C., & Lambert, D. L. 2007, *A&A*, 465, 271
- Ramírez, I., Allende Prieto, C., Redfield, S., & Lambert, D. L. 2006, *A&A*, 459, 613
- Ramírez, I., Asplund, M., Baumann, P., Meléndez, J., & Bensby, T. 2010, *A&A*, 521, A33
- Ramírez, I., Meléndez, J., & Asplund, M. 2009, *A&A*, 508, L17
- Reddy, B. E., Tomkin, J., Lambert, D. L., & Allende Prieto, C. 2003, *MNRAS*, 340, 304
- Roederer, I. U., Lawler, J. E., Sneden, C., Cowan, J. J., Sobeck, J. S., & Pilachowski, C. A. 2008, *ApJ*, 675, 723
- Sadakane, K., Ohkubo, M., & Honda, S. 2003, *PASJ*, 55, 1005
- Schuler, S. C., Flateau, D., Cunha, K., King, J. R., Ghezzi, L., & Smith, V. V. 2011, *ApJ*, 732, 55
- Serenelli, A. M., Haxton, W. C., & Pena-Garay, C. 2011, *ArXiv e-prints*
- Simmerer, J., Sneden, C., Cowan, J. J., Collier, J., Woolf, V. M., & Lawler, J. E. 2004, *ApJ*, 617, 1091
- Sneden, C. A. 1973, PhD thesis, The University of Texas at Austin
- Takeda, Y. 2005, *PASJ*, 57, 83
- Takeda, Y., Kawanomoto, S., Honda, S., Ando, H., & Sakurai, T. 2007, *A&A*, 468, 663
- Tull, R. G., MacQueen, P. J., Sneden, C., & Lambert, D. L. 1995, *PASP*, 107, 251
- Turcotte, S., & Wimmer-Schweingruber, R. F. 2002, *Journal of Geophysical Research (Space Physics)*, 107, 1442
- Turner, N. H., ten Brummelaar, T. A., McAlister, H. A., Mason, B. D., Hartkopf, W. I., & Roberts, Jr., L. C. 2001, *AJ*, 121, 3254
- Udry, S., & Santos, N. C. 2007, *ARA&A*, 45, 397
- van Leeuwen, F. 2007, *A&A*, 474, 653
- Weidenschilling, S. J. 1977, *Ap&SS*, 51, 153
- Yi, S., Demarque, P., Kim, Y., Lee, Y., Ree, C. H., Lejeune, T., & Barnes, S. 2001, *ApJS*, 136, 417
- Yi, S. K., Kim, Y., & Demarque, P. 2003, *ApJS*, 144, 259
- Zhang, H. W., Gehren, T., & Zhao, G. 2008, *A&A*, 481, 489